

# A COORDINATED POWER CONTROL STRATEGY COMBINED FUEL CELL/ELECTROLYZER/ SUPER-CAPACITOR/BATTERY POWER GENERATION AND GRID INTEGRATION

Syed Zulqadar Hassan<sup>\*1</sup>, Hui Li<sup>1</sup>, Tariq Kamal<sup>2</sup>, Izhar Hussain<sup>3</sup>, Amin Khan<sup>4</sup>, María Jesús Espinosa- Trujillo<sup>5</sup>, Asif Kabir<sup>1</sup>

<sup>1</sup>State Key Laboratory of Power Transmission Equipment and System Security and New Technology, School of Electrical Engineering, Chongqing University, Chongqing, China

<sup>2</sup>Department of Electrical and Electronics Engineering, Sakarya University, Faculty of Technology, Serdivan/Sakarya, Turkey

<sup>3</sup>VLSI Laboratory, Department of Electronics and Telecommunication Engineering, Politecnico di Torino, Italy

<sup>4</sup>Electrical Engineering Department, University of Engineering and Technology, Peshawar, Pakistan

<sup>5</sup>Universidad Tecnológica Metropolitana, 115 404, Santa Rosa, Mérida 97279, Yucatán, México

\*Corresponding Author: syedzulqadar.hassan.pk@ieee.org

cqulh@163.com, tariq.kamal.pk@ieee.org, izhar.hussain@polito.it, engr.amenkhan@gmail.com, mjesus@hotmail.com, asifkabir@cqu.edu.cn

**ABSTRACT:** Fuel Cell (FC) offers various benefits such as fuel flexibility, high efficiency, green power modularity and cogeneration options. However, FC fails in providing fast response and also faces load following problems. Since, an integration of FC with complementary device such as a Super-capacitor (SC) or battery can offer an alternate power generation option. This manuscript provides a Coordinated Power Control Strategy (CPCS) for a hybrid power generation which consists of a FC, an Electrolyzer (ELYZ), a SC and a battery that support local grid or grid integrated load. According to the proposed strategy, the FC is utilized the primary energy source. The SC is used as a complement and/or backup device to balance the slow dynamic response of FC during transient. The battery is utilized as a high energy density and/or backup device to stabilize the DC-bus voltage while the ELYZ used as a dump load during surplus power. The CPCS works in two layers. The first layer managed the overall power management system. Depending upon load demand, this layer generates references to the second layer. The second layer controls the individual subsystems i.e., FC, ELYZ, SC and battery according to the references coming from the first layer. The dynamic performance of the proposed system is checked under real-world record load conditions at Peshawar, Pakistan. The effectiveness of the proposed model in term of voltage regulation, power transfer, load tracking and grid stability is verified by Matlab simulation results.

**Keywords:** Fuel cell, Hybrid storage system, Coordinated Control Strategy, Stability and power quality analysis.

## INTRODUCTION

Nowadays, pollutants in the atmosphere are progressing in parallel with the increasing demand of energy. The continuous increasing demand for fossil fuels such as natural gas, crude oil and coal is motivating society towards the development of Renewable Energy Sources (RES) power generation. Many RES, such as solar photovoltaic systems, hydro power systems, hydrogen FC power systems and wind power systems are polluted free and abundantly available [1-5]. Among all, FC technology for grid enhancement has exposed its significant potential and consider an indispensable energy source for the future power system [6]. The FC is a static energy source that generates electricity from hydrogen through electrolysis. The superior reliability, with practically zero noise level or no moving parts is an extra advantage of FC system as compared to the diesel generator.

There are several types of FCs which are classified on the basis of their operating temperature ranges and type of electrolyte. In this study, Solid Oxide Fuel Cell (SOFC) is selected, because, it works at high temperatures (800 – 1000 °C) [7]. This makes SOFC the highest efficiency FC among others [6], [8], [9]. Some special characteristics, like internal reforming or larger fuel flexibility, very fast kinetics reaction without platinum catalysts and tolerance to impurities make the performance of SOFC better among all FCs [10]–[12]. Other advantages of SOFC are the distributed configurations, cogeneration options and reusability of heat in bottoming cycle. Despite high efficiency and flexibility, there are some weaknesses in SOFC. One common drawback in all FCs is their slow dynamic load tracking capabilities [13]. When a SOFC is subjected to a large power fluctuations, it experiences an instant

drop off of the voltage in the I-V curve and take several seconds to deliver the required power. In the meantime, hydrogen starvation can occur which results the detrimental of cell life and efficiency [14]. The problem of slow dynamic response of SOFC can be addressed through a high energy density device such as SC or battery. Therefore, it is essential to operate SOFC under steady state condition. Without SC or battery, the SOFC power system must meet all the power demand, which consequently increases the size and cost of the SOFC power plant.

Various FC based hybrid generation systems are discussed in the literature. For example, in [15]–[19], the authors explained the control of various hybrid systems including FC, SC and battery. In [15], [16], the authors designed a FC power generation with SC storage for electric vehicle applications. In both studies the authors explained the combine benefit of FC and UC. The modeling and power control for hybrid power topology including FC/SC is simulated in [17]. In [18], the author designed a FC/ battery hybrid system through adaptive control scheme. The advantages of the FC generation as a green technology is appear in [19]. Control and simple energy management scheme for a photovoltaic/SC/battery hybrid system is developed in [20]. In [21], the importance of FC storage system in photovoltaic/SC hybrid power plant is discussed. Energy management of wind with hydrogen and battery storage system is developed in [22]. In all these studies, majority of the authors work on polymer electrolyte membrane fuel cell while some authors support their research work on the basis of virtual weather pattern. In all these studies, majority of the authors work on polymer electrolyte membrane fuel cell. This paper offers a coordinated power control approach combining SOFC, ELYZ, SC, battery and a set of residential

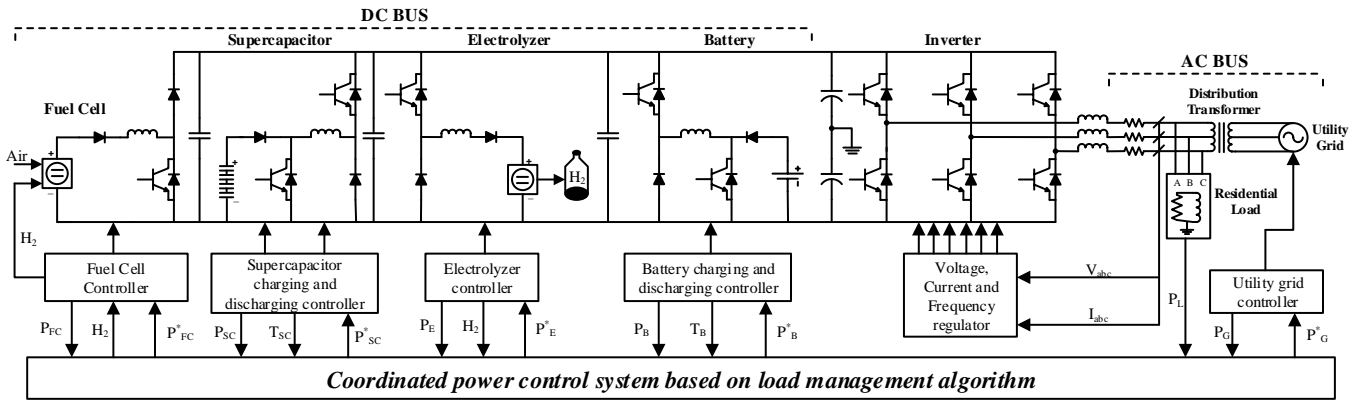


Figure 1: Configuration of proposed hybrid power system

loads for grid on and grid off applications. The proposed test bed works on CPCS. The CPCS managed the overall power management system for the proposed system and control all the individual subsystem on the basis of dynamic references. The CPCS ensures premium quality and reliability of power for the 24 Hrs simulation.

This paper is structured as follows. First, an overall system configuration is provided in Section 2. Section 3 explains the modeling of system components. Section 4 presents the control of individual components. Section 5 hosts the CPCS. Simulation results and conclusions are described in Section 6 and 7.

### SYSTEM CONFIGURATION

It is possible to accomplish much higher generating capacity factors by an integrating FC stack and with a hybrid storage configuration to overcome the fluctuations in plant output. An efficient energy storage scheme is required to get continuous and constant power, and the electrical power delivered by the FC stack has to be converted into SC or battery energy. Figure 1 explains the configuration of proposed hybrid system which consists of a 50 kW SOFC stack as prior energy source. A 58 F SC and 50 Ah battery hybrid storage system are in the proposed architecture to use as a high energy density and/or backup energy source. A pressurized 50 kW alkaline electrolyze is used as dump as a load during surplus power to generate hydrogen which is stored in hydrogen tank for later use in the SOFC stack.

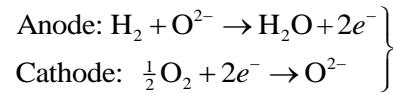
The four subsystems i.e., FC, ELYZ, SC and battery are controlled through four separate control units. All the subsystems are combined in parallel to a common DC bus through their individual non-isolated DC converters. The output of DC bus is then integrated to the grid or grid connected load through an inverter. All the energy sources and their controllers are designed in Matlab/Simulink. The complete hybrid system is simulated for 24 Hrs including different operating and load conditions under CPCS supervision. The simulation results conclude the operating principle and effectiveness of this proposed system. It is essential to point out that the architecture of proposed system is modular and thus easily expandable as long as a new FC, SC or battery are added to the existing ones with no need to increase the circuit and control complexity. Furthermore, it is also possible to upgrade the existing system by adding another parallel inverter. Thus, the proposed system is beneficial for distributed energy generation.

### SYSTEM MODELING FORMULATION

This section explains the dynamic modeling of the individual components involved in the proposed system.

#### SOFC Modeling

The model used in this study is based on the dynamic SOFC model explained in [23], [24]. During modeling, diffusion phenomena of hydrogen and oxygen gases, constant stable operating temperature and the double layer charging effect are considered. The chemical reactions occur at respective electrodes is written as



The dynamics of the reactant's partial pressure associated in the system can be expressed as

$$\left. \begin{aligned} \frac{V_1}{RT_{FC}} \frac{d}{dt} p_{\text{H}_2} &= r_{\text{H}_2}^{\text{in}} - r_{\text{H}_2}^{\text{out}} - \frac{I_{FC}}{2F} \\ \frac{V_2}{RT_{FC}} \frac{d}{dt} p_{\text{H}_2\text{O}} &= r_{\text{H}_2\text{O}}^{\text{in}} - r_{\text{H}_2\text{O}}^{\text{out}} - \frac{I_{FC}}{2F} \\ \frac{V_3}{RT_{FC}} \frac{d}{dt} p_{\text{O}_2} &= r_{\text{O}_2}^{\text{in}} - r_{\text{O}_2}^{\text{out}} - \frac{I_{FC}}{4F} \end{aligned} \right\} \quad (1)$$

where  $V_j$ s refer to the number of volumes of electrode side,  $p_j$  represents the partial pressure of  $j$ th species ( $j= \text{H}_2, \text{H}_2\text{O}, \text{O}_2$ ),  $R$  and  $F$  stand for gas constant and Faraday constant, respectively.  $r_j$  is the mass flow rate of  $j$ th species,  $I_{FC}$  is FC current.

Depending on the chemical reaction occur at cathode and anode, the voltage developed in a cell ( $V_{cell}$ ) can be expressed in (2) according to Nernst equation.

$$V_{cell} = E_{cell} - \sum V_{\text{losses, cell}} \quad (2)$$

with

$$E_{cell} = E_{o, cell} - k_B(T_{FC} - 298) + \frac{RT_{FC}}{2F} \ln \left\{ \frac{p_{\text{H}_2} \sqrt{p_{\text{O}_2}}}{p_{\text{H}_2\text{O}}} \right\} \quad (3)$$

$$V_{FC} = N_{cell} V_{cell}, P_{FC} = V_{FC} I_{FC}$$

where  $E_{cell}$  is the Nernst's voltage,  $E_{o, cell}$  stands for Gibbs potential,  $N_{cell}$  is the number of cells in the FC stack,  $T_{FC}$  is the operating temperature,  $P_{FC}$  is power delivered from FC, and  $k_B$  is Boltzmann constant. Remember that  $E_{cell}$  in (3) expressed

reactants' partial pressure dynamics and value of pressures in (1) are derived under open circuit voltage condition. The individual potential drop term in (2) can be written in (4).

$$\left. \begin{aligned} \sum V_{losses,cell} &= V_{a,cell} + V_{c,cell} + V_{o,cell} \\ V_{a,cell} &= \lambda_0 + (T_{FC} - 298)x + T_{FC}y \ln I_{FC} \\ V_{c,cell} &= -\frac{RT_{FC}}{cF} \ln \left( 1 - \frac{I_{FC}}{I_l} \right) \\ V_{o,cell} &= R_o I_{FC} \end{aligned} \right\} \quad (4)$$

where  $V_{c,cell}$  is concentration potential,  $V_{a,cell}$  is cell-activation potential,  $V_{o,cell}$  is ohmic potential drop.  $\lambda_0$ ,  $x$ ,  $y$ , and  $R_o$  are parameters of FC and  $I_{FC}$  is the current of FC and  $I_l$  is the limiting current. To provide the require voltage and power level, a FC stack is modeled according to the parameters given in the Appendix.

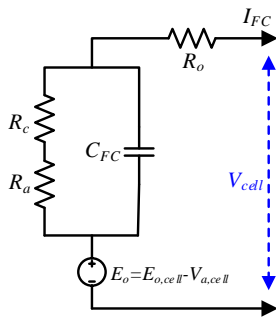
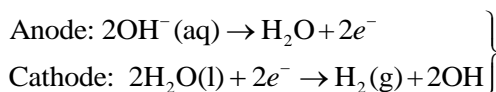


Figure 2: Equivalent electrical model of fuel cell

Figure 2 shows the electrical model of FC explaining the three regions i.e., activation loss occurs due to the starting of chemical reaction inside in FC, voltage drop due to flow resistance of ions in the electrolyte is the middle of the curve is an ohmic loss (approximately linear), and voltage drop due to the mass transfer inside the porous media is concentration loss.

**Electrolyzer Modeling**

ELYZ is a static electrochemical device, which consume water and heat to generate hydrogen and oxygen, and technically classified as the opposite of FC system. The modeling of ELYZ involves different dynamics: the hydraulic dynamic, electrochemical dynamic, thermal dynamic and electrical dynamic. The thermal modeling is omitted in this paper and constant temperature approach is adopted considering the large time constant of the thermal model. Here, the potassium hydroxide (KOH) i.e., alkaline ELYZ model is taken and as proposed in [5], [25]–[27]. The chemical reactions occur in the ELYZ is written as



In (5), Faraday's explains molar hydrogen production rate as a function of applied current.

$$r_{H_2,p} = \beta(T_E, J_E) \frac{N_E}{2F} I_E \quad (5)$$

where  $N_E$  and  $T_E$  represents the number of cells in a FC stack and temperature of the ELYZ, respectively. The Faraday

efficiency,  $\beta$  in term of current density ( $J_E$ ) and temperature is written in (6).

$$\left. \begin{aligned} \beta &= \frac{J_E^2}{z_1 + J_E^2} z_2 \\ z_1 &= 50 + 2.5T_E, \quad z_2 = 1 - 7.5 \times 10^{-4} T_E \end{aligned} \right\} \quad (6)$$

The electrical dynamic of the ELYZ is established upon the empirical parameters whose values are taken from the experiments. The V–I characteristics of the ELYZ can be written in (7) and (8) by nonlinear and empirical relationship as

$$v_{cell} = v_0 + I_E(r_1 + r_2 T_E) / A_E + v_1 \log((k_1 + k_2 / T_E + k_3 / T_E^2) / A_E + 1) \quad (7)$$

$$V_E = N_E v_{cell} \quad (8)$$

where  $v_0$  is the thermodynamic potential of FC,  $v_{cell}$  is the voltage drop across ELYZ. Note that  $v_0$  is the function pressure and temperature.  $r_i$ s are the parameters of ohmic resistance, and  $v_1$  and  $k_i$ s represent the parameters for the ELYZ over voltage. The values of all parameters are given in the Appendix. During designing rated FC stack, it is assumed that both no-load voltages of ELYZ and SOFC are equal. Broadly speaking by doing  $N_{cell} E_{cell} = N_E v_0$ , there would be continuous static phase for FC/ELYZ unit. Thus, smooth transition happens between two modes i.e., FC mode and ELYZ mode.

The hydraulic part of an ELYZ contains the dynamics of the resultant gases. Considering the ideal gas law, the dynamics of resultant pressure can be defined as

$$\frac{V'_E}{RT_E} \frac{d}{dt} p_{H_2,e} = r_{H_2,p} - r_{H_2,o} \quad (9)$$

where  $r_{H_2,p}$  and  $r_{H_2,o}$  are the molar hydrogen production rate, and molar hydrogen outflow rate, respectively.  $\hat{V}_E$  is the cathode volume, and  $p_{H_2,e}$  is the partial pressure of hydrogen associated with cathode. Under steady state,  $r_{H_2,p} = r_{H_2,o}$  must be satisfied to keep constant pressure.

**Compressor and Hydrogen Tank Modeling**

Based on polytropic model, the compressor power is expressed in term of hydrogen molar flow rate using (10)

$$\left. \begin{aligned} r_{H_2,o} &= \frac{\gamma_c}{\alpha} P_{comp} \\ \alpha &= \frac{dRT_E}{d-1} \left[ \left( \frac{p_t}{p_E} \right)^{\frac{d-1}{d}} - 1 \right] \end{aligned} \right\} \quad (10)$$

where  $\gamma_c$  stands for compression efficiency,  $p_t$  is the pressure of hydrogen tank, and  $\alpha$  is the polytropic work. Furthermore, the pressure of store hydrogen depends on the difference between input and output flow rates, and express in the following differential equation [28],

$$\frac{V_t}{RT_t} \frac{d}{dt} p_t = r_{H_2,o} - r_{H_2}^{in} \quad (11)$$

where  $T_i$  and  $V_i$  are the temperature and the volume of hydrogen inside the tank, respectively.

**Super-capacitor Modeling**

This study works on the classical SC model provide in Figure 3, which consists of a double-layer capacitance ( $C$ ), and two resistances, viz., an equivalent parallel leakage resistance ( $R_p$ ), and an equivalent charging/discharging series resistance ( $R_s$ ) [29].

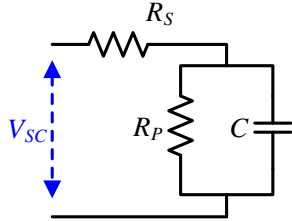


Figure 3: Equivalent electrical model of SC

The amount of energy consumed/drawn from the SC bank ( $E_{SC}$ ) depends on the capacitance of SC and the potential develop across its terminals, given by

$$E_{SC} = \frac{1}{2} C (V_{initial}^2 - V_{final}^2) \tag{12}$$

When the SC is subjected to release energy, the magnitude of terminal voltage across SC is decreased and vice versa. To provide the required voltage level, multiple numbers of SC modules are joined in series and/or parallel configuration. All the parameters of the SC are given in Appendix

**Battery Modeling**

The battery model consists of two RC circuits as proposed in [30], [31] and shown in Figure 4. The two voltages ( $e_a, e_b$ ) across two capacitances ( $C_a, C_b$ ) and the state of charge ( $T_B$ ) are three state variables of the battery. The open circuit voltage ( $V_{oc}$ ) and the value of resistance can be defined in (13).

$$\left. \begin{aligned} V_{oc} &= 338.8 \times [0.94246 + 0.05754 \times T_B] \\ R_a C_a \frac{de_a}{dt} + \left( \frac{R_a + R_a}{R_a} \right) \cdot e_a &= V_{oc} + \frac{R_a}{R_a} \cdot e_a \\ R_b C_b \frac{de_b}{dt} + e_b &= e_b - R_b I_t \end{aligned} \right\} \tag{13}$$

The battery SOC ( $T_B$ ) is an indication of the energy reserve and is written as

$$T_B = 100 \left( 1 - \frac{\int I_B dt}{Q_{max}} \right) \% \tag{14}$$

$I_B$  is the battery current and determined using (15)

$$I_B = \frac{V_{oc} - \sqrt{V_{oc}^2 - 4(r+r_1)P}}{2(r+r_1)} \tag{15}$$

where  $r$  and  $r_1$  represent the internal and polarization resistance of battery.  $Q_{max}$  and  $P$  represents the maximum battery charge (Ah) and output power (W) of the battery, respectively.

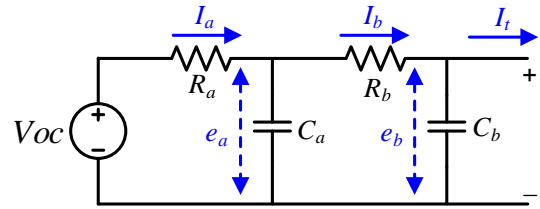


Figure 4: Equivalent electrical model of battery

**CONTROL OF SYSTEM COMPONENTS**

This section describes the control and power electronics interfacing of individual components system.

**Control System of SOFC**

The output voltage or power of SOFC depends upon load demand, and the increase in load demand decreases its voltage or power. Therefore, a DC-DC boost converter is applied at the SOFC system to maintain the DC bus output voltage constant i.e., 700V. The boost controller is controlled though a conventional Proportional Integral Differentiator (PID) controllers. The PIDs work on the error, which is the difference between the measured voltage and actual voltage of SOFC. Based on the error, the PID adjusts the duty cycle according to the requirement. The control system for SOFC is depicted in Figure 5.

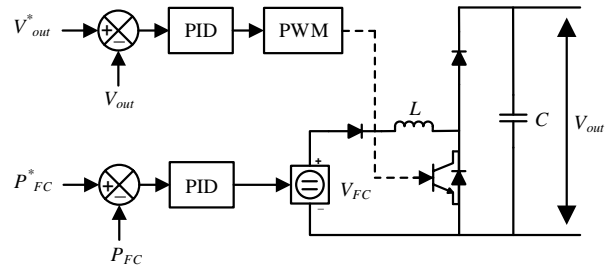


Figure 5: Control system of fuel cell

**Control System of Electrolyzer**

The output power of ELYZ is controlled by controlling its input current [32], [33]. A buck converter is used to regulate the input current of ELYZ which consequently control the output power. The buck converter is itself controlled by a Proportional Integral (PI) controllers. The control system for ELYZ is shown in Figure 6.

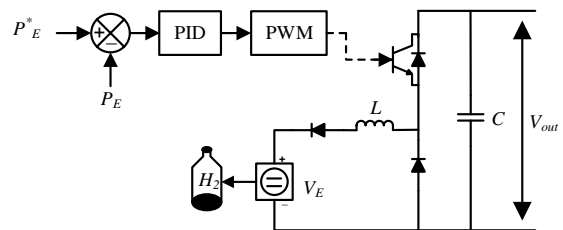


Figure 6: Control system of ELYZ

**Control System of Super-capacitor/Battery**

The control strategy is developed for both SC and battery on the basis of their charging and discharging capabilities. The output voltage or power of SC and/or battery is always smaller than the DC bus voltage. A boost converter is used to increase the output voltage SC and/or battery to the desire value i.e.,

700 V. Similarly, a buck converter is used to charge the SC and/or battery from DC bus under CPCS. The buck-boost converter is itself controlled by PID controller. Due to an inner control loops, SC and/or battery must follow (16). The control system for SC/battery is shown in Figure 7.

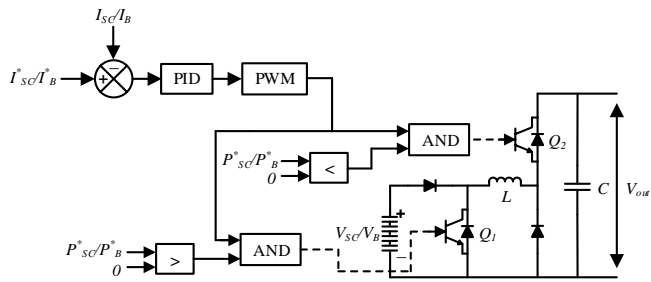


Figure 7: Control system of SC/battery

$$I^* = P^* / V^* \tag{16}$$

$I^*$  is reference current, and  $P^*$ ,  $V^*$  are the reference power and reference voltage, respectively.

### Control System of Grid Connected Inverter

Figure 8 explains the basis control strategy of the proposed three phase inverter connecting the DC bus voltage of the hybrid system to the grid and/or grid-connected load. The inverter operates on power conversion from the DC bus voltage of the hybrid system to the grid and/or grid-connected load, and also regulates the grid current at unity power factor. The current controlled inverter is controlled to provide sinusoidal current after filtering, which is fed to the utility line to distribute the required power. It also stabilizes the DC bus voltage. The inverter increases the output power when the DC bus voltage is increased and vice versa. The proposed control technique uses PI controllers and hysteresis current control pulse width modulation technique to generate suitable gate signals for driving the controllable switches of the inverter.

The inputs to PI controllers are the errors calculated between the measure and actual values of the active and the reactive powers. The PI controllers try to diminish the error in order to achieve the desired active and the reactive powers. Furthermore, it is desirable for the grid current to be controlled in phase with the grid voltage and have unity power factor. To perform such function, the phase angle of the grid voltage is calculated through phase locked loop. The grid current is controlled using outer current control loop through PI voltage controller while the unity power factor is adjusted using inner current control loop through PI current controller as defined in (17) and (18).

$$I_{L\_ref} = k_{pv} (V_{dc\_ref} - V_{dc}) + k_{iv} \int (V_{dc\_ref} - V_{dc}) dt \tag{17}$$

$$I_{L\_ref} = k_{pi} (I_{ref} - I_L) + k_{ii} \int (I_{ref} - I_L) dt \tag{18}$$

where  $k_{pv}$ ,  $k_{iv}$ ,  $k_{pi}$  and  $k_{ii}$  are the gains of the PI voltage and PI current controllers,  $I_{L\_ref}$  is the reference current of grid,  $V_{dc}$ ,  $I_L$ ,  $V_{dc\_ref}$  and  $I_{ref}$  are the DC bus actual voltage, DC bus actual current, DC bus reference voltage and DC bus reference current, respectively.

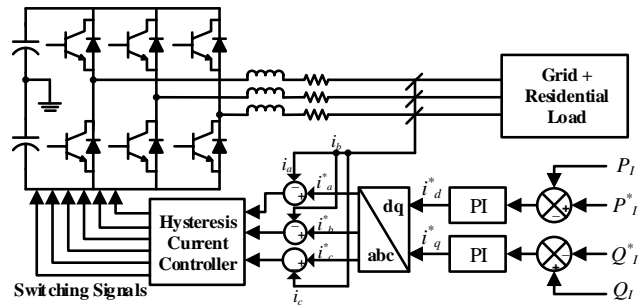


Figure 8: Control system of grid connected inverter

### COORDINATED POWER CONTROL STRATEGY (CPCS)

The CPCS ensures optimal use and energy management of SOFC, SC, battery and even grid. The CPCS generates the dynamic references for each subsystem which confirms: 1) continuity of power 2) energy management of storage systems 3) tracking of loads for 24 Hrs and 4) reducing burden on the grid.

#### 5.1. Load Arrangement

Based on available renewable energy sources, the power balance equation for proposed HPS can be written as follows

$$P_{FC} = P_L \pm P_B \pm P_{SC} \pm P_G + P_E \tag{19}$$

where  $P_L$ ,  $P_{SC}$ ,  $P_B$ ,  $P_G$  and  $P_E$  are the load demand, SC output power, battery output power, utility grid output power and ELYZ power consumption, respectively. The excess power generated by FC ( $P_{EX}$ ) is utilized by battery, SC, utility grid and ELYZ as follows

$$P_{EX} = P_L - P_{FC} = -(P_B + P_{SC} + P_E + P_G) \tag{20}$$

Whereas, due to maximum power limitation of FC, the shortage of power ( $P_S$ ) is supplied by SC, battery and utility grid, respectively as follows.

$$P_S = P_L - P_{FC} = P_{SC} + P_B + P_G \tag{21}$$

Based on above power balance equations, a load management algorithm is presented in Figure 9 in which following conditions are incorporated.

- The use of power produced by the FC system has priority in satisfying load demand over that delivered by the SC/battery system or grid.
- If the power produced by FC system is higher than the demand, the excess power is used to charge the SC or battery bank. If still excess power is available, then it will be sent to the grid. If still excess power is available, then it will be used for electrolysis to generate hydrogen for later use in FC.
- Similarly, if the total power generated by the FC system is less than the demand, power will be delivered from the battery bank. If the load demand exceeds the power generated by the FC/Battery combination, the difference is supplied by the SC. If still load demand is not satisfying then grid's power will be used to fill the gap. If still demand is not satisfied then load shedding is executed.

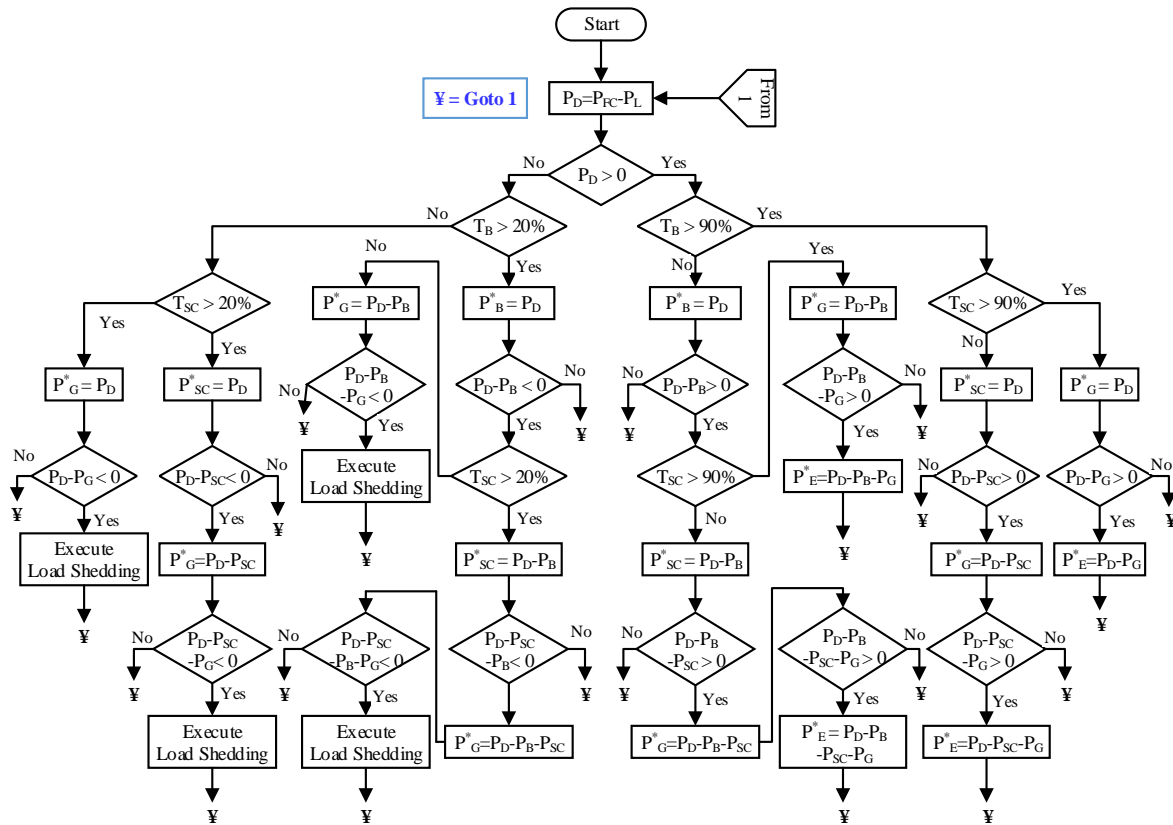


Figure 9: Flow chart of load management algorithm

The CPCS is based on an above load management algorithm. For better understanding, the operation of CPCS is organized in the modes described in table 1 and discussed as follow.

**Mode 1 to 4**

The primary condition for modes is that the load is less than the maximum power rating of FC. Hence the overall demand is satisfied by FC itself. Mode 1 and 2 contains the off grid condition. In mode 1, due to slow response of FC, the FC does not fulfill the sudden changed demand and that deficient power is supplied by battery and SC. Whereas in the same fashion in mode 2, the sudden change in load demand is fulfilled by battery and excess power is system is absorbed by SC and ELYZ. Mode 3 and 4 contain NRHG and RHG, respectively. In NRHG, the grid supports the FC and fulfil the power deficiency, whereas in RHG the grid act as a load and draw power from FC.

**Mode 5 to 8**

The primary condition remains the same that the load demand is less than the maximum power rating of FC. In mode 5, grid and SC are disconnected and only the battery assists the FC. In mode 6, due to NRHG, the grid along with battery supports the FC during rapid change in load. In mode 7, the power generated by FC is greater than the load and off-grid condition. Hereafter, the excess power is consumed by battery and SC. In mode 8, FC and grid (NRHG) produce power more than load demand. The excess power is distributed among battery and SC as per algorithm.

**Mode 9 to 12**

Alike previous mode the load demand is less than the maximum power rating of FC. In mode 9, due to RHG, the

grid also acts as a load and draw power from FC while the excess power generated by FC is used to charge battery and SC. Similarly, in mode 10, the grid is disconnected and excess power is solely consumed by the battery. In mode 11 and 12, the grid is at NRHG and RHG conditions, respectively whereas in both the cases the excess power is utilized by battery only.

**Mode 13 to 17**

After mode 12, the primary condition is changed that the load demand is greater than the maximum power rating of FC. Therefore, other energy sources like battery, SC and grid are used to fulfil the deficient power. In mode 13, the grid is detached and battery/SC achieves the remaining power deficiency. Similarly, is mode 14 and 15, the grid is at NRHG and RHG conditions. During NRHG condition, the grid supports the battery/SC to accomplish the power deficiency, whereas in RHG condition, the grid also acts as a load on battery/SC. In mode 16 and 17, the grid is disconnected. Moreover, the difference between the two modes is only the consumption strategy. In mode 16, the shortage of power is supplied by battery only while in mode 17, the battery not only fulfills the deficiency, but also produce some excess power, which is consumed by SC.

**Mode 18 to 22**

In mode 18 and 19, the grid is at NRHG and RHG condition, respectively. In both modes, the battery generates more power than deficiency and this excess power is consumed by SC. The only difference is these modes are of grid condition that the grid helps battery in mode 18 and act a load in mode 19.

Table 1: Operating modes of CPCS

Mode	Primary condition	Secondary condition	Tertiary condition
1			$P_D=P_B+P_{SC}$
2		Off grid (OG)	$P_D=P_B-P_{SC}$
3		Non-rush hour of grid (NRHG)	$P_D=P_B-P_{SC}+P_G$
4		Rush hour of grid (RHG)	$P_D=P_B-P_{SC}-P_G$
5	$P_L < P_{FC-MAX}$	OG	$P_D=P_B$
6		NRHG	$P_D=P_B-P_G$
7		OG	$P_D=-P_B-P_{SC}$
8		NRHG	$P_D=-P_B-P_{SC}+P_G$
9		RHG	$P_D=-P_B-P_{SC}-P_G$
10		OG	$P_D=-P_B$
11		NRHG	$P_D=-P_B+P_G$
12		RHG	$P_D=-P_B-P_G$
13		OG	$P_D=P_B+P_{SC}$
14		NRHG	$P_D=P_B+P_{SC}+P_G$
15		RHG	$P_D=P_B+P_{SC}-P_G$
16	$P_L > P_{FC-MAX}$	OG	$P_D=P_B$
17		NRHG	$P_D=P_B-P_{SC}+P_G$
18		RHG	$P_D=P_B-P_{SC}-P_G$
19		OG	$P_D=-P_B-P_{SC}$
20		NRHG	$P_D=-P_B+P_G$
21		RHG	$P_D=-P_B-P_G$
22		NRHG	$P_D=-P_B+P_G$

Last three modes i.e., mode 20, 21 and 22, are exceptional modes. These modes exist for a very short time. This mode exists only when a load is changed suddenly nearly equal to the maximum power rating of FC, then the FC output power overshoots and  $P_{FC}$  become greater than  $P_L$  (although  $P_L < P_{FC-MAX}$ ). At this stage the battery and SC consume the excess power. In mode 20 and 21, the grid is isolated. In mode 20, only the battery consumes the excess power where in mode 21 the excess power is shared between battery and SC. Similarly, in mode 22, due to NRHG condition, the excess power generated by FC plus grid power which is totally utilized by battery for charging.

**SIMULATION, RESULTS AND DISCUSSION**

For validation of proposed algorithm and performance of CPCS, the proposed architecture is tested in Matlab/Simulink. Using the simpower system, the simulations are performed for different load conditions. The parameters used in modeling of FC, battery, SC, ELYZ, grid and inverter are presented in Appendix. The proposed system provides power to residential load of a small community at Peshawar, Pakistan. The peak load and average load are calculated as 2.8 kW and 2.02 kW per home, respectively. The peak load starts from 18 Hrs and ends at 21 Hrs. The simulation results of all the modes are discussed below.

Figure 10 shows the time versus operating mode generated by CPCS. Between 1-8 and 16-18 Hrs, the  $P_L < P_{FC-MAX}$ , so, the operating modes lies between 0-12. Similarly, for remaining duration, the operating mode lies above 13.

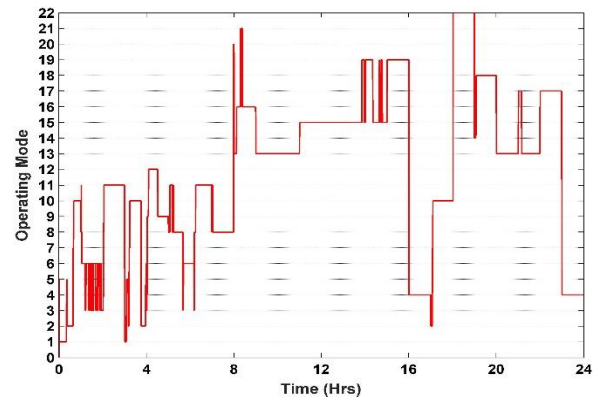


Figure 10: Time versus operating mode

Figure 11 shows the simulation results of output and reference powers of residential load, grid, FC, battery, SC and electrolyzer for t=0-3 Hrs. From Figure 11(a), the solid blue line shows the actual residential load before load shedding (P-WLS) whereas dotted black and solid red lines shows the reference and actual residential loads after execution of load shedding. The phenomenon of load shedding is incorporated due to shortage of power from energy sources which is clearly revealed from Figure 11. However, at t=2-3 Hrs, the load is fully satisfied by FC/SC/battery and no need of load shedding. Figure 11(b) shows the reference and actual power supplied by the grid. Similarly, from Figures 11(c), (d) and (e) represents the reference and actual powers of FC, battery and SC, respectively. The ELYZ consumes any excess power generated by energy sources to keep system stable as shown in Figure 11 (f). Throughout Figure 11, the positive value of power represents that the energy source is supplying power and vice versa.

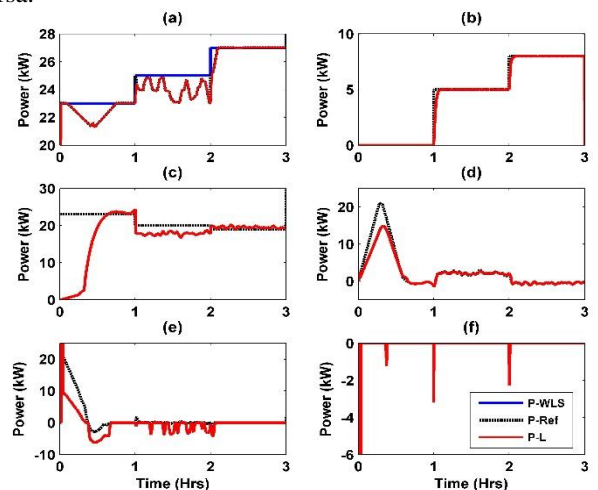


Figure 11: Simulation results for t=0-3 Hrs (a)  $P_L$  (b)  $P_G$  (c)  $P_{FC}$  (d)  $P_B$  (e)  $P_{SC}$  (f)  $P_E$

Figure 12 represents the simulation results of different energy sources for a duration of 3-6 Hrs. It is clearly revealed from Figure 12(a) that for a short period of time load shedding is needed. All the load demand is satisfied with the collaboration of FC/SC/battery as shown in Figure 12(c), (d) and (e). After 5 Hrs, grid also supports FC to overcome the load demand and any excess present inside the system is consumed by ELYZ as illustrated in Figure 12 (b) and (f). In this interval, the CPCS varies from 1 to 11 operating modes.

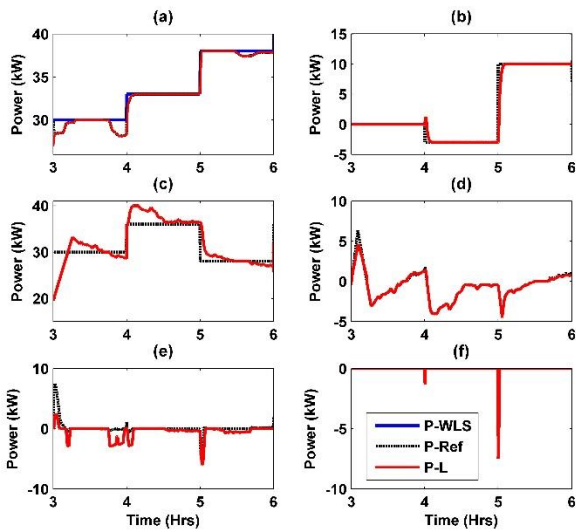


Figure 12: Simulation results for t=3-6 Hrs (a)  $P_L$  (b)  $P_G$  (c)  $P_{FC}$  (d)  $P_B$  (e)  $P_{SC}$  (f)  $P_E$

From 6-9 Hrs interval, both of the primary conditions exist. The rated power of FC is 50 kW, while the maximum power provided by FC is 55 kW. From Figure 13 (a), the load demand varies from 43 kW to 53 kW. Above 50 kW, i.e., after 8 Hrs, the second primary condition is started. FC provides its maximum power to satisfy the load demand and the remaining load demand is satisfied by battery as shown in Figures 13 (c) and (d). From Figure 13 (e), due to slow response of FC at rapidly changing load at 8 Hrs, the SC attempts to fulfil the power gap by using its power density property. On the other side, the utility grid assists FC and ELYZ play its role to keep the system stable as depicted in Figures 13 (b) and (f). Due to existence of both primary conditions, the CPCS also shifts between 8 to 21 operating modes.

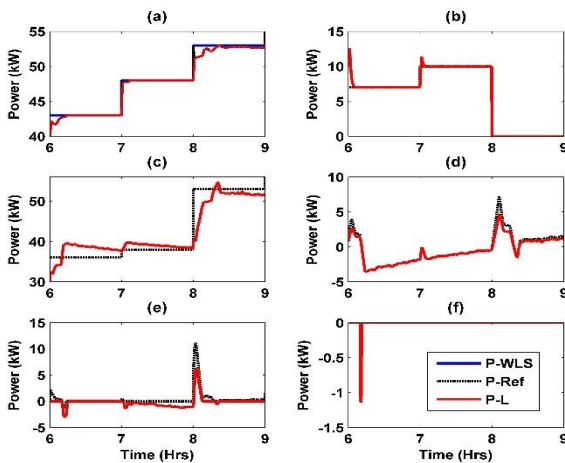


Figure 13: Simulation results for t=6-9 Hrs (a)  $P_L$  (b)  $P_G$  (c)  $P_{FC}$  (d)  $P_B$  (e)  $P_{SC}$  (f)  $P_E$

For a duration of 9-12 Hrs, the residential load demand is greater than the rated power of FC and FC delivers its maximum power of 50 kW as shown in Figures 14 (a) and (c). Hence, the battery, grid and SC endeavors to satisfy the remaining load demand, but from Figures 14 (b), (d) and (e), they are unable to meet their reference power. Therefore, a load shedding is executed as shown in Figure 14 (a). In this

interval, due to shortage of power there is no excess power in the system and ELYZ power consumption is zero as presented in Figure 14 (f).

For a period of 12-15 Hrs, the residential load demand is again greater than the rated power of FC as shown in Figure 15(c). Therefore, CPCS generates the remaining power references to grid, battery and SC to overcome the power shortage. From Figure 15, the battery, SC and grid almost accomplish the power gap except 13-13.2 Hrs in which it is necessary to execute load shedding. Since, battery also produces some excess power at 14 Hrs which is successfully utilized by ELYZ as shown in Figure 15 (f). As  $P_L > P_{FC-MAX}$ , the CPCS fluctuates in between 13 to 19 operating mode as shown in Figure 10.

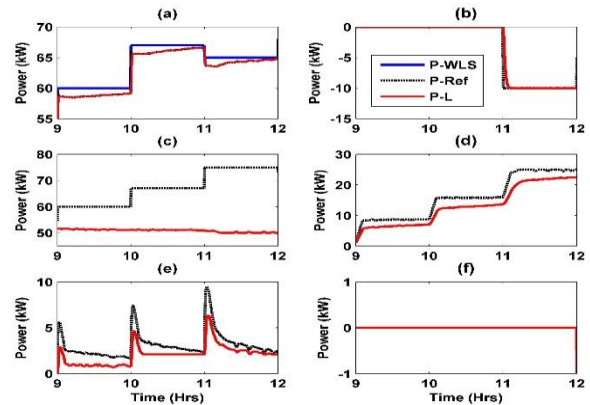


Figure 14: Simulation results for t=9-12 Hrs (a)  $P_L$  (b)  $P_G$  (c)  $P_{FC}$  (d)  $P_B$  (e)  $P_{SC}$  (f)  $P_E$

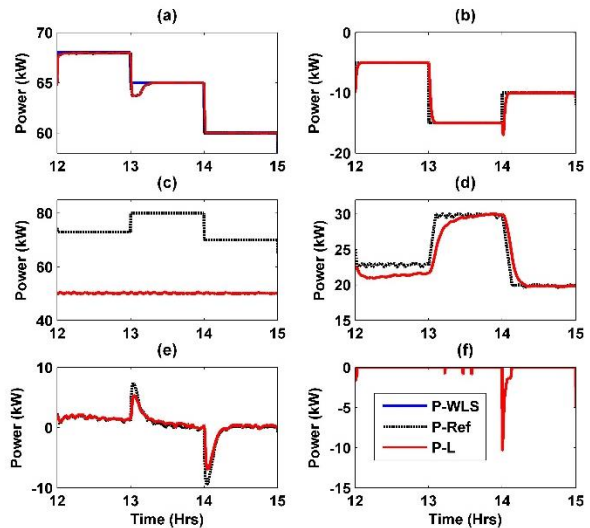


Figure 15: Simulation results for t=12-15 Hrs (a)  $P_L$  (b)  $P_G$  (c)  $P_{FC}$  (d)  $P_B$  (e)  $P_{SC}$  (f)  $P_E$

From Figure 16, the load demands vary from 53 kW to 43 kW. In this interval both the primary conditions exist. Accordingly, the FC delivers its maximum power and deficient power is satisfied by battery, SC and grid as shown in Figure 16. In this case, all the energy sources efficiently fulfil the load demand. So, there is no need of load curtailment. Some excess power is generated in system during load changes, which is properly disposed-off by electrolyzer system as shown in Figure 16 (f).

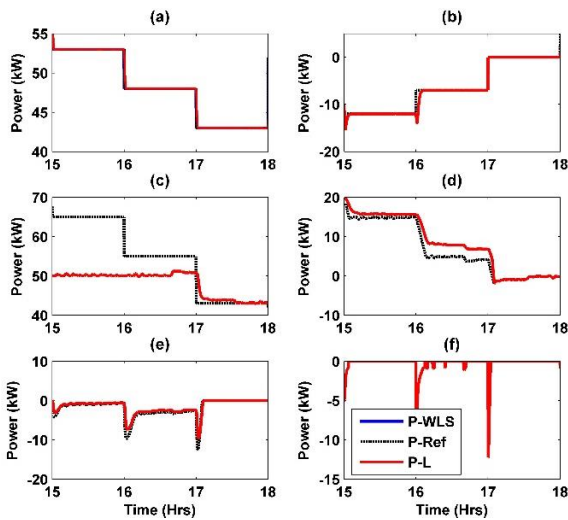


Figure 16: Simulation results for t=15-18 Hrs (a) PL (b) PG (c) PFC (d) PB (e) PSC (f) PE

Between 18-24 Hrs,  $P_L > P_{FC-MAX}$  as shown in Figures 17(a) and 18(a). Due to rush hour of grid, it also act as a load. Hence, FC supplies its maximum power of 50 kW and the shortage of about 0-20 kW of power is supplied by battery and SC as shown in Figures 17 and 18. Due to nonfulfillment of load demand at certain points (especially when the load is changing), the load curtailment is executed.

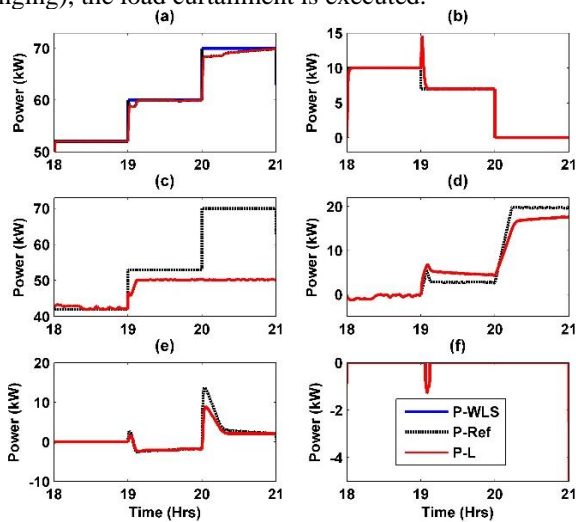


Figure 17: Simulation results for t=18-21 Hrs (a) PL (b) PG (c) PFC (d) PB (e) PSC (f) PE

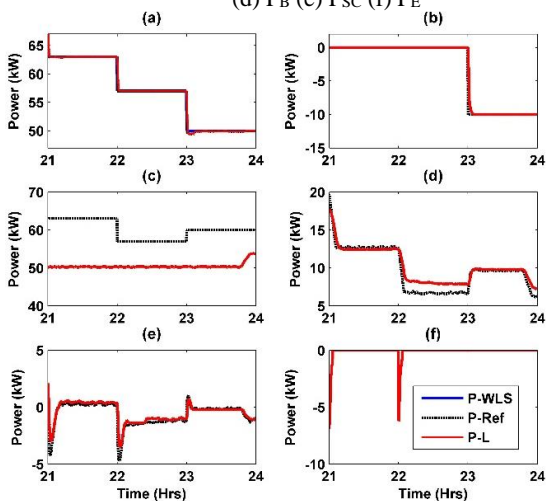


Figure 18: Simulation results for t=21-24 Hrs (a) PL (b) PG (c) PFC (d) PB (e) PSC (f) PE

Figure 19 shows the overall load shedding executed by CPCS for entire 24 Hrs. Usually, it is executed when residential load demand changes (at every hour). Due to efficient load management algorithm, CPCS kept the load curtailment below 2 kW. On the other side, the SOCs of battery and SC are shown in Figure 20. Battery is discharging most of the time while SC is both charging and discharging depending upon the power available.

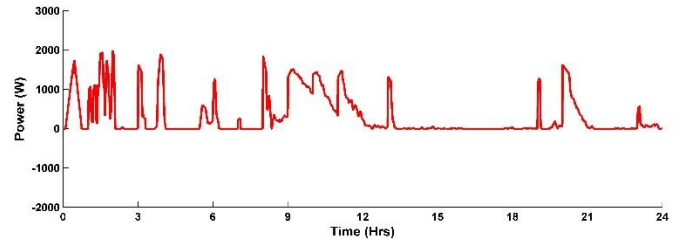


Figure 19: Load shedding executed vs time

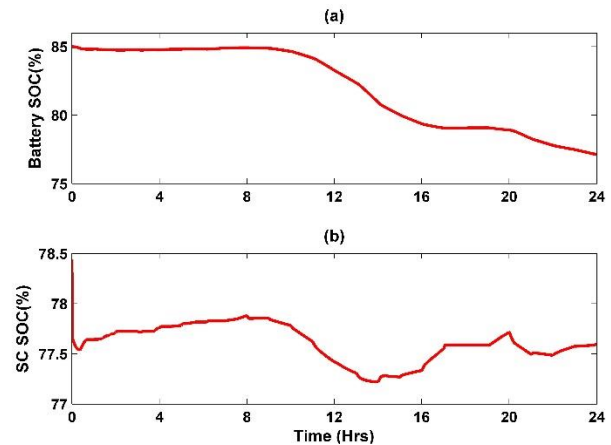


Figure 20: State of charge (a) Battery (b) SC

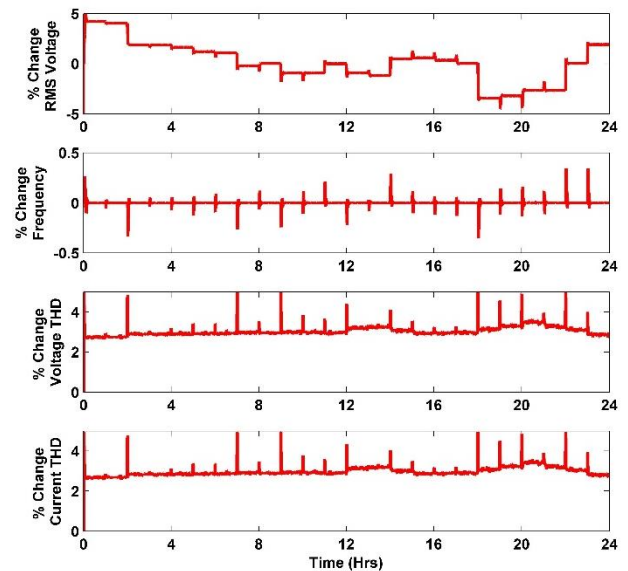


Figure 21: Power quality parameters

Since, all the electrical equipment are highly sensitive, so, the power quality is a serious concern. Power quality is particularly addressed in proposed CPCS, which is clearly shown in Figure 21. Load voltage frequency, RMS load voltage and THD for load voltage and current are all in their

acceptable limits [34], which ensures that the system provides quality power.

The system is said to be a stable one when all the power inside it is zero. If a system contains real power, then it alters the line-to-line voltage of the load while if a system contains reactive power, it alters the frequency of load voltage. From Figure 22, it is clearly revealed that the net power on both DC and AC busses are zero and the system is called as stable.

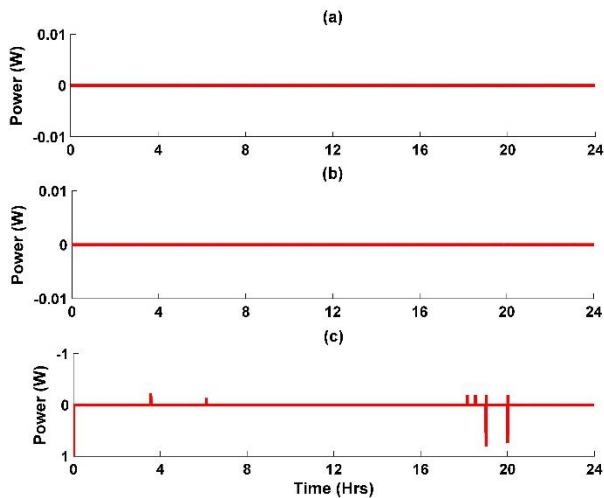


Figure 22: System stability parameters (a) Net power on DC bus (b) Net real power on AC bus (c) Net reactive power on AC bus

## CONCLUSION

An optimal control strategy for a hybrid power system with different energy storage system for a grid on and grid off applications is presented. The drawback of a single power source i.e., FC is addressed by proposing a hybrid energy storage system. A complete simulation model of FC/ELYZ/SC/battery has been prepared which facilitates the grid and/or grid connected load under the supervision of CPCS. The proposed system shows excellent dynamic performance in term of power sharing, grid stability, power quality and reliability which has been verified by the simulations performed in Matlab/Simulink.

## APPENDIX

### a) Electrical Network

$$V_{DC} = 700 \text{ V}, V_{L-L,rms} = 440 \text{ V}, f = 50 \text{ Hz}, P_{G,rated} = 10 \text{ MVA}$$

### b) SOFC

$$P_{rated} = 50 \text{ kW}, T_{FC} = 1173 \text{ K}, N_{cell} = 325, \text{ Stack} = 4 \text{ kW}$$

$$\text{Array size} = 13, T_d = 5 \text{ s}, F = 96484.6 \text{ C/mol}$$

### c) Battery (CINCOFM/BB12100T)

$$\text{Capacity} = 200 \text{ Ah}, \text{ Voltage/string} = 12 \text{ V}, N_p = 3, N_s = 34,$$

$$V_{rated} = 12 \times 34 \approx 408 \text{ V}$$

### d) SC (Maxwell Technologies BMOD0058)

$$C = 58 \text{ F}, V_{max} = 16.2 \text{ V}, \text{ ESR} = 22 \text{ m}\Omega, I_{max} = 20 \text{ A}, I_{leakage} = 1$$

$$\text{mA}, N_p = 20, N_s = 6.$$

### e) Electrolyzer (QualeanQL-85000)

$$P_{E,rated} = 50 \text{ kW}, v_o = 1.038 \text{ V}, A_E = 0.25 \text{ m}^2, c = 2, N_E = 350,$$

$$k_1 = -1.002 \text{ A}^{-1} \text{ m}^2, k_2 = 8.424 \text{ A}^{-1} \text{ m}^2 \text{ }^\circ\text{C}, k_3 = 247.3 \text{ A}^{-1} \text{ m}^2 \text{ }^\circ\text{C}^2,$$

$$v_l = 0.185 \text{ V}, r_l = 8.05 \times 10^{-5} \Omega \text{ m}^2, r_2 = -2.5 \times 10^{-7} \Omega \text{ m}^2$$

## ACKNOWLEDGMENT

The research work is supported by National Natural Science Foundation of China (No. 51377184), International Science & Technology Cooperation Program of China (No.2013DFG61520) and Fundamental Research Funds for the Central Universities (No. CDJZR12150074).

## REFERENCES

- [1] Y. Kim and S. Kim, "An electrical modeling and fuzzy logic control of a fuel cell generation system," *IEEE Trans. Energy Convers.*, **14**(2):239–244(1999).
- [2] D. P. Papadopoulos and J. C. Dermentzoglou, "Economic viability analysis of planned WEC system installations for electrical power production," *Renew. Energy*, **25**(2): 199–217(2002).
- [3] M. Zahran, "Photovoltaic hybrid systems reliability and availability," *J. Power Electron.*, **3**(3): 145–150(2003).
- [4] C. Rubbia, "Today the world of tomorrow—The energy challenge," *Energy Convers. Manag.*, **47**(17): 2695–2697(2006).
- [5] T. Zhou and B. Francois, "Modeling and control design of hydrogen production process for an active hydrogen/wind hybrid power system," *Int. J. Hydrogen Energy*, **34**(1): 21–30(2009).
- [6] S. Hoseinnia and S. M. Sadeghzadeh, "A Comparative Study of Fuel Cell Technologies and their Role in Distributed Generation," in *IEEE EUROCON 2009*, 464–469(2009).
- [7] T. Das and S. Snyder, "Adaptive control of a solid oxide fuel cell ultra-capacitor hybrid system," in *Proceedings of the 2011 American Control Conference*, 3892–3898(2011).
- [8] S. Giddey, S. P. S. Badwal, A. Kulkarni, and C. Munnings, "A comprehensive review of direct carbon fuel cell technology," *Prog. Energy Combust. Sci.*, **38**(3): 360–399(2012).
- [9] S. Mekhilef, R. Saidur, and A. Safari, "Comparative study of different fuel cell technologies," *Renew. Sustain. Energy Rev.*, **16**(1): 981–989(2012).
- [10] J. Larminie, A. Dicks, and M. S. McDonald, *Fuel cell systems explained*, vol. 2. Wiley New York, 2003.
- [11] X. Li, L. Fields, and G. Way, "Principles of fuel cells," *Platin. Met. Rev.*, **50**(4): 200–201(2006).
- [12] M. H. Nehrir and C. Wang, *Modeling and control of fuel cells: distributed generation applications*, John Wiley & Sons, **41**(2009).
- [13] J. R. Meacham, F. Jabbari, J. Brouwer, J. L. Mauzey, and G. S. Samuelsen, "Analysis of stationary fuel cell dynamic ramping capabilities and ultra capacitor energy storage using high resolution demand data," *J. Power Sources*, **156**(2): 472–479(2006).
- [14] P. Thounthong and P. Sethakul, "Analysis of a Fuel Starvation Phenomenon of a PEM Fuel Cell," in *2007 Power Conversion Conference - Nagoya*, 731–738(2007).
- [15] P. Rodatz, G. Paganelli, A. Sciarretta, and L. Guzzella, "Optimal power management of an experimental fuel cell/supercapacitor-powered hybrid vehicle," *Control Eng. Pract.*, **13**(1): 41–53(2005).
- [16] V. Paladini, T. Donato, A. de Risi, and D. Laforgia, "Super-capacitors fuel-cell hybrid electric vehicle optimization and control strategy development," *Energy Convers. Manag.*, **48**(11): 3001–3008(2007).
- [17] M. Uzunoglu and M. S. Alam, "Dynamic modeling, design and simulation of a PEM fuel cell/ultra-capacitor hybrid system for vehicular applications," *Energy Convers. Manag.*, **48**(5): 1544–1553(2007).
- [18] Z. Jiang, L. Gao, and R. A. Dougal, "Adaptive Control Strategy for Active Power Sharing in Hybrid Fuel Cell/Battery Power Sources," *IEEE Trans. Energy Convers.*, **22**(2): 507–515(2007).
- [19] K. Rajashekara, "Hybrid Fuel-Cell Strategies for Clean Power Generation," *IEEE Trans. Ind. Appl.*, **41**(3): 682–689(2005).
- [20] S. Z. Hassan, H. Li, T. Kamal, S. Mumtaz, L. Khan, and I. Ullah, "Control and Energy Management Scheme for a PV/SC/Battery Hybrid Renewable Power System," *Sci. Int.*, **28**(2): 955–964(2016).
- [21] T. Kamal, S. Z. Hassan, M. J. Espinosa-Trujillo, H. Li, and M. Flota, "An optimal power sharing and power control strategy of photovoltaic/fuel cell/ultra-capacitor hybrid power system," *J. Renew. Sustain. Energy*, **8**(3): 035301(2016).
- [22] T. Kamal, S. Z. Hassan, H. Li, S. Mumtaz, and L. Khan, "Energy

- management and control of grid-connected wind/fuel cell/battery Hybrid Renewable Energy System,” in *2016 International Conference on Intelligent Systems Engineering (ICISE)*, 161–166(2016).
- [23] M. H. Nehrir, “A Physically Based Dynamic Model for Solid Oxide Fuel Cells,” *IEEE Trans. Energy Convers.*, **22**(4): 887–897(2007).
- [24] S. Z. Hassan, H. Li, T. Kamal, S. Mumtaz, and L. Khan, “Fuel Cell/Electrolyzer/Ultra-capacitor hybrid power system: Focus on integration, power control and grid synchronization,” in *2016 13th International Bhurban Conference on Applied Sciences and Technology (IBCAST)*, 231–237(2016).
- [25] O. Ulleberg, “Modeling of advanced alkaline electrolyzers: a system simulation approach,” *Int. J. Hydrogen Energy*, **28**(1): 21–33(2003).
- [26] P. Artuso, R. Gammon, F. Orecchini, and S. J. Watson, “Alkaline electrolyzers: Model and real data analysis,” *Int. J. Hydrogen Energy*, **36**(13): 7956–7962(2011).
- [27] T. Kamal, “Adaptive Control of Fuel Cell and Design of Power Management System (PMS) for PHEVs/EVs Charging Station in a Hybrid Power System,” MS Thesis, COMSATS Institute of Information Technology Abbottabad-Pakistan, 2014.
- [28] T. Kamal, S. Z. Hassan, H. Li, and M. Awais, “Design and power control of fuel cell/electrolyzer/microturbine/ultra-capacitor hybrid power plant,” in *2015 International Conference on Emerging Technologies (ICET)*, 1–6(2015).
- [29] O. C. Onar, M. Uzunoglu, and M. S. Alam, “Modeling, control and simulation of an autonomous wind turbine/photovoltaic/fuel cell/ultra-capacitor hybrid power system,” *J. Power Sources*, **185**(2): 1273–1283(2008).
- [30] L. Gao, Z. Jiang, and R. A. Dougal, “An actively controlled fuel cell/battery hybrid to meet pulsed power demands,” *J. Power Sources*, **130**(1–2): 202–207(2004).
- [31] A. Hajizadeh and M. A. Golkar, “Control of hybrid fuel cell/energy storage distributed generation system against voltage sag,” *Int. J. Electr. Power Energy Syst.*, **32**(5):488–497(2010).
- [32] S.-K. Kim, J.-H. Jeon, C.-H. Cho, J.-B. Ahn, and S.-H. Kwon, “Dynamic Modeling and Control of a Grid-Connected Hybrid Generation System With Versatile Power Transfer,” *IEEE Trans. Ind. Electron.*, **55**(4): 1677–1688(2008).
- [33] C. Singh, “Multicriteria Design of Hybrid Power Generation Systems Based on a Modified Particle Swarm Optimization Algorithm,” *IEEE Trans. Energy Convers.*, **24**(1): 163–172(2009).
- [34] “IEEE Standard for Interconnecting Distributed Resources with Electric Power Systems,” *IEEE Std 1547-2003.*, 1–28(2003).